

A Comparison of Nonlinear Combustion Stability Methods

Jonathan C. French*

Software and Engineering Associates, Inc., Carson City, NV 89701

Despite many decades of study, new solid rocket motor systems frequently experience unsteady gas motions and associated motor vibrations. This phenomenon most often occurs when the acoustic modes of the combustion chamber couple with combustion/flow processes. Current linear models of the sort used in the Standard Stability Prediction program (SSP) are designed to predict the tendency for a SRM to become unstable, but they do not provide any information on the *severity* of the instability, usually measured by the limit cycle amplitude of the oscillations. Software and Engineering Associates, Inc. (SEA) has endeavored to implement two nonlinear numerical models for combustion stability analysis that predict limiting amplitudes. In this paper, we compare and contrast the capabilities of these two models. Also, the numerically predicted oscillatory behavior of the acoustic pressure in the limit cycle is examined for different stability scenarios to develop an understanding of the oscillatory motions inside solid rocket motors.

Nomenclature

\bar{a}	=	Speed of sound
k	=	Frequency parameter
L	=	Length of combustion chamber
p'	=	Acoustic pressure
P	=	Chamber pressure
\bar{r}	=	Spatial coordinate
s	=	Perturbed entropy
t	=	Time
u'	=	Acoustic velocity
\bar{u}	=	Steady velocity
V	=	Combustion chamber volume
x	=	Axial position (0 at head end)
α_n	=	Linear stability integral
$\bar{\gamma}$	=	Ratio of specific heats
ε	=	Limit cycle amplitude
θ_n	=	Phase shift
$\bar{\rho}$	=	Mean density
η	=	Temporal acoustic mode function
ψ_m	=	Spatial acoustic mode function
ω_n	=	Natural frequency

Subscripts

m, n = Acoustic mode numbers

Copyright © 2006 by Software and Engineering Associates, Inc. Published by the American Institute of Aeronautics and Astronautics, Inc., with permission.

* Senior Research Engineer, AIAA member

I. Introduction

Solid rocket motor combustion stability analysis has historically focused on the linear stability problem to predict whether or not a solid rocket motor will be stable or unstable. In an effort to predict the severity of an instability, we have encoded two nonlinear combustion stability models into our design tools, a gas dynamics module and an energy balance module. While these two methodologies have distinctly different origins,^{1,2} they have been shown to yield similar maximum peak oscillatory pressures (limit cycle amplitudes) for a simple cylindrical motor design.³ Herein, we compare the results between the two methodologies for two grain design configurations and a variety of linear stability parameters.

The combustion stability analyses presented were computed using SEA's Solid Performance Program (SPP) solid rocket motor design code. In 1976, Aerojet developed the Standard Stability Prediction (SSP) code, which SEA subsequently incorporated as a module within SPP. This allows SPP to feed the motor geometry data and chamber ballistics to the SSP program as a function of web burn with minimal user intervention. The linkage enables the user to evaluate the linear stability of a motor over the entire burn for a user specified number of resonant frequencies, with a minimum amount of user intervention to set up each test case.

The two nonlinear analyses both require a determination of the linear stability as part of the solution process. The gas dynamics approach is designed to evaluate the nonlinear behavior of the acoustic motions at a given point in time, without taking into account the continued burning of the propellant. As the oscillatory pressures typically quickly enter a limit cycle, this does not usually cause a problem in the determination of the severity of the problem. The gas dynamics approach allows the amplitudes of the different acoustics modes to change in time until equilibrium is reached.

In contrast, the energy balance approach presumes that the relative amplitudes of the acoustic waves are fixed relative to one another, such that the overall acoustic motion represents a sawtooth wave. Alternately, it is possible to utilize the amplitudes obtained by the gas dynamics approach to compute the relative weights for the energy balance approach. The amplitude of the sawtooth wave is allowed to change with time. The energy balance approach removes energy from the dynamic system by computing the entropy gain across the traveling sawtooth wave's steep front. The associated stability integrals were rederived to accommodate the mean chamber pressure. If the mean flow field is separated from the perturbed flow field by time averaging instead of a quasi-steady assumption, Flandro noted that the origin of the DC shift may be revealed. As the assumption of the relative wave magnitudes greatly reduces the complexity of the problem, the energy balance approach was incorporated into SPP's main ballistics algorithm, allowing the stability and the mean chamber ballistics to interact over the duration of the motor burn. This paper focuses on the limit cycle amplitude and neglects the DC shift, as the DC shift cannot be computed with the current gas dynamics formulation.

While it has been demonstrated that the two approaches yield similar results for a cylindrical test case, it is the objective of this paper to compare the limit cycle amplitude and overall acoustic motions for a variety of chamber geometries. As the energy balance is mainly a function of only the unstable mode's linear stability parameter, we investigated how changes in the stable modes' stability parameters change limit cycle amplitudes. The overall acoustic motion in a realistic motor geometry was evaluated, and an unusual and unanticipated acoustic motion is presented.

II. Approach

It is the overall goal of this paper to compare the results obtained by the gas dynamics and the energy balance approaches. As the limit cycle for the energy balance can be computed without time integration, most of the computational efforts will be focused on evaluating the gas dynamics approach, and then comparing the computed limit cycle amplitudes with those predicted by the energy balance approach.

A. Gas Dynamics Approach

The Gas Dynamics approach utilizes separation of variables directly. We have followed the formulation from Burnley⁴ in developing our SPP/SSP implementation. The partial differential equation of interest is the wave equation:

$$\frac{1}{\bar{a}^2} \int \psi_n \frac{\partial^2 p'}{\partial t^2} dV + k_n^2 \int \psi_n p' dV = - \int \psi_n h dV - \oint \psi_n f dS \quad (1)$$

Separation of variables is used to define the pressure as the sum of the product of the mode shape and its time varying function:

$$\frac{p'(\bar{r}, t)}{\bar{p}} = \sum_{m=1}^{\infty} \eta_m(t) \psi_m(\bar{r}) \quad (2)$$

$$u'(\bar{r}, t) = \sum_{m=1}^{\infty} \frac{\dot{\eta}_m(t)}{\bar{\gamma} k_m^2} \nabla \psi_m(\bar{r}) \quad (3)$$

The mode shapes (ψ) are already known. Thus, solving for η :

$$\frac{\partial^2 \eta_n}{\partial t^2} + \omega_n^2 \eta_n = -\frac{\bar{a}^2}{\bar{p} E_n^2} \left\{ \int \psi_n h dV - \oint \psi_n f dS \right\} \quad (4)$$

The parameters h and f contain the first and second order gas dynamics terms which drive the system of equations:

$$h = -\bar{\rho} \nabla \cdot \left(\bar{u} \cdot \nabla u' + u' \cdot \nabla (\bar{u} - u') - \frac{p'}{\bar{\gamma} \bar{p}} \frac{\partial u'}{\partial t} \right) + \frac{1}{\bar{a}^2} \bar{u} \cdot \nabla \frac{\partial p'}{\partial t} \quad (5)$$

$$+ \frac{\bar{\gamma}}{\bar{a}^2} \frac{\partial p'}{\partial t} \nabla \cdot \bar{u} + \frac{1}{\bar{a}^2} \frac{\partial}{\partial t} (u' \cdot \nabla p') + \frac{\bar{\gamma}}{\bar{a}^2} \frac{\partial}{\partial t} (p' \nabla \cdot u') + \nabla \cdot F' - \frac{1}{\bar{a}^2} \frac{\partial P'}{\partial t}$$

$$f = \bar{\rho} \left(\frac{\partial u'}{\partial t} + \bar{u} \cdot \nabla u' + u' \cdot \nabla \bar{u} + u' \cdot \nabla u' \right) \cdot \hat{n} + \frac{p'}{\bar{a}^2} \frac{\partial u'}{\partial t} - F' \cdot \hat{n} \quad (6)$$

The first order terms comprise the linear stability terms. When the first order terms are approximated with equations (2) and (3), the integrals of the product of two mode shapes (equation (4)) yield the Kronecker delta, because the mode shapes are orthogonal in space. The first order terms have only one time function, and as such are linear and may be placed on the left hand side (LHS). However, when the second order terms are approximated with equations (2) and (3), the product of three mode shape functions are integrated in space, yielding a third order tensor dotted with two time function vectors. These two time function vectors represent the non-linear portion of the ODE, and are placed on the right hand side (RHS) to drive the linear LHS:

$$\ddot{\eta}_n - 2\alpha_n \dot{\eta}_n + (\omega_n^2 - 2\omega_n \theta_n) \eta_n = -\sum_{i=1}^{\infty} \sum_{j=1}^{\infty} [A_{nij} \dot{\eta}_i \dot{\eta}_j + B_{nij} \eta_i \eta_j] \quad (7)$$

A_{nij} and B_{nij} are 3rd order tensors which contain all the spatial effects (some terms have been presumed to be small and thus neglected):

$$A_{nij} = \frac{1}{E_n^2} \int \left[\frac{1}{\bar{\gamma} k_i^2} (\nabla \psi_i \cdot \nabla \psi_j + \bar{\gamma} \psi_j \nabla^2 \psi_i) \psi_n + \frac{1}{\bar{\gamma} k_i^2 k_j^2} [(\nabla \psi_i \cdot \nabla) \nabla \psi_j] \cdot \nabla \psi_n \right] dV \quad (8)$$

$$B_{nij} = -\frac{1}{E_n^2} \int \left\{ \frac{\bar{a}^2}{\bar{\gamma}} [(\nabla \psi_i \cdot \nabla \psi_j + \bar{\gamma} \psi_i \nabla^2 \psi_j) \psi_n + \psi_i \nabla \psi_j \cdot \nabla \psi_n] \right\} dV \quad (9)$$

The simplest approach to solving this system of equations (7) is to determine the stability alphas (α_n) and phase shifts (θ_n) using SSP, imparting an initial amplitude for the unstable mode, and then integrating forward in time. The response functions required to compute the phase shifts are difficult to obtain experimentally. However, we have used random values for this parameter with minimal difference in the limit cycle amplitudes, implying this is not a critical parameter.

B. Energy Balance Approach

The energy balance approach is similar, but contains a significant assumption: the final form of the overall wave motion is a steep fronted traveling wave.^{5,6} The Fourier coefficients are selected to be a sawtooth wave front. Therefore, rather than allowing the spectral components to float towards a final solution, each is given a weight relative to the first mode. The only unknown is the overall amplitude of the summation of the modes. Rather than refer to the wave equation, Flandro implements an energy balance with sources of energy from the linear instability, such as pressure coupling, and a primary non-linear sink, identified as the entropy gain across the steep fronted wave, as originally derived by Temkin.⁷ The rate of energy dissipation across the steep wavefront (for a perfect gas) is:

$$\frac{\partial E_{steep\ wavefront}}{\partial t} = A_{CS} \frac{\gamma + 1}{2} \frac{(\Delta p')^3}{6\rho_0^2 c_0^3} \quad (10)$$

$\Delta p'$ is the jump in the perturbed pressure across the steep wavefront. The motivation for this approach was to ensure that this entropy loss is incorporated into the solution, and to simplify the analysis procedure. Time integration of a larger system of ODEs is no longer needed. Simplification of the problem also allows one to better understand the underlying physics of the problem. For a cylindrical motor, the energy balance, written in terms of the steep fronted waveform's amplitude, can be written as:

$$\frac{d\varepsilon}{dt} = \varepsilon\alpha_1 - \varepsilon^2 \left(\frac{\gamma + 1}{6\gamma} \right) \frac{\bar{a}}{L} \quad (11)$$

wherein L is the cylinder length, \bar{a} is the speed of sound, γ is the ratio of the specific heats, and α_1 is the first mode's stability parameter. In the limit cycle, this predicts that the system amplitude is linearly proportional to the unstable mode's stability parameter:

$$\varepsilon = \frac{\alpha_1}{\left(\frac{\gamma + 1}{6\gamma} \right) \frac{\bar{a}}{L}} \quad (12)$$

A steep-fronted wave can form in an unstable motor to dissipate energy from the acoustic-combustion feedback loop. The available energy loss is due to a gain in entropy across the steep wave front. Please note that we are not claiming this is the only way energy can be removed – there are other nonlinear energy sinks available such as particle damping. The observed FFT amplitudes of experimental data are often the Fourier decomposition of a steep-fronted wave form. The unstable mode drives the system, and the fluid responds by generating a larger, overall motion that acts to remove energy from the system. This steep-fronted wave can be approximated by a traveling shock wave.

A traveling shock wave can be formulated as an infinite sum of acoustic mode shapes. The shock wave strength was previously derived by Morfey and Temkin, and Flandro.^{5,6} A more current derivation was presented recently by Flandro et al, yielding the first acoustic mode amplitude as a function of the shock wave strength.

Flandro has derived a particular solution that satisfies the jump in entropy across a steep-fronted wave:

$$\frac{s_2 - s_1}{c_v} = \frac{\gamma^2 - 1}{12\gamma^2} \left(\frac{p'_{shock\ amplitude}}{P} \right)^3 + O(p'_{shock\ amplitude}{}^4) \quad (13)$$

The pressure amplitude of the normalized shock wave Fourier decomposition is:

$$p'_{shock\ amplitude} = \varepsilon(t) \sum_m \frac{2}{m\pi} \psi_m(x) \sin(m\omega_1 t) \quad (14)$$

By choosing the sawtooth wave form, both the Fourier amplitudes and phase shifts of each mode are specified. In contrast to the gas dynamics system of equations approach, the sawtooth wave form presumes the amplitude of each mode relative to the fundamental mode amplitude remains constant. Only the overall system amplitude (ε) need be computed. Another subtle corollary is that the temporal frequency is specified to be an integer multiple of the fundamental frequency. While we are assuming that the higher modes are “forced” and are not oscillating at their harmonic frequency, this does not apply to the spatial frequency. The spatial frequency must remain constant as otherwise the mode shapes would not each satisfy the spatial boundary conditions. We verified the temporal assumption both experimentally and computationally (with the gas dynamics approach) in Ref. 3.

If one assumes the pressure oscillations enter a sawtooth wave form in the limit cycle, one can postulate not only what the axial mode looks like, but also the radial and tangential modes. The traveling axial sawtooth wave shape is simply:

$$p'(x,t) = \sum_n \frac{1}{n} \cos\left(\frac{n\pi}{L} x\right) \sin\left(\frac{n\pi}{a_0 L} t\right) \quad (15)$$

This yields a traveling steep-fronted wave, as in Figure 1. The x direction is the axial position in the motor, and the y direction represents the acoustic pressure amplitude.

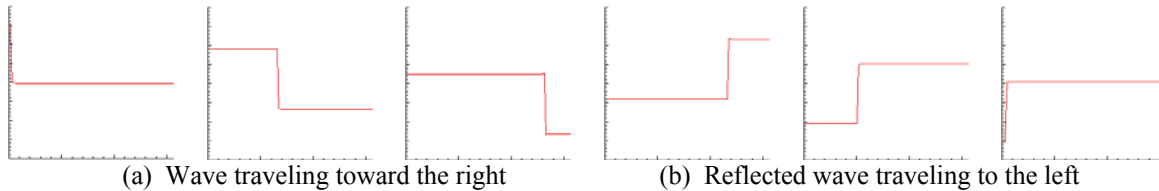


Figure 1. Traveling axial shock wave

It should be emphasized here that the assumption of a sawtooth wave contrasts with the previous gas dynamics analysis in which the overall motion was allowed to grow to its final form with respect to time. The energy balance approach allows us to not only arrive at an answer sooner, but it also provides a physical interpretation of the nonlinearity along with the means to evaluate the effect of the instability on the mean (or slowly varying) physical properties. It is not as flexible as the gas dynamics / system of equations approach, as it does not handle unusual situations. For example, when the second mode is unstable, the gas dynamics approach yields two traveling steep-fronted waves with only the even acoustic modes excited.

In a numerical experiment, we evaluated the limit cycle amplitude of a combustion instability event in a cylindrical solid rocket motor using a CFD approach,⁸ and the gas dynamics and energy balance approximate methods. In order to compare the amplitudes from gas dynamics with the energy balance approach, we digitized the peak amplitudes from Refs. 1 and 8, as shown in Figure 2. We ran our implementation of the gas dynamics approach in SSP, and the peak amplitudes corresponded with the results from Culick and Yang. Evaluation of both Flandro's 1985 energy balance analysis and his recent formulations proved favorable, and the latest computations match exactly with the Baum and Levine result.

One of the benefits of using the Baum and Levine test case is the given values for the linear stability analysis. The response function is precisely defined, rather than experimentally derived. It is interesting to note here that in the Culick and Yang analysis, the analysis only matched the Baum and Levine results when the flow turning stability integral was ignored. This matches a recent derivation by Flandro that demonstrated that the flow turning integral was an artifact of an early irrotational assumption in the linear stability analysis derivation.

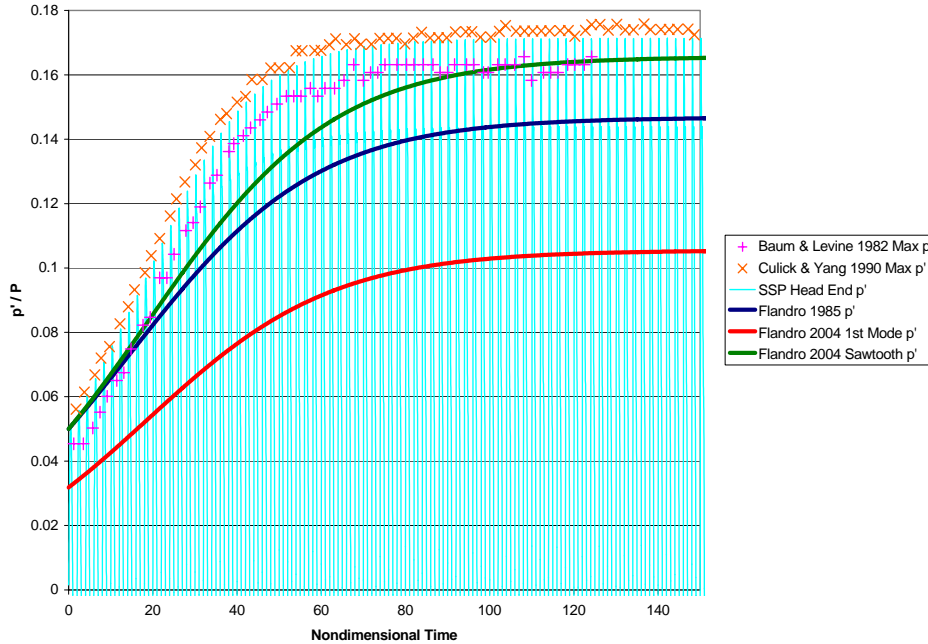


Figure 2. Comparison of different nonlinear methods

III. Results

As shown in Figure 2, the gas dynamics and energy balance approaches yield similar results for a simple cylinder. To compare these two approaches further, we will test three different situations, two with a simple cylinder, and one with a more complicated grain design.

A. Cylindrical Motor, Varied Stable Mode Stability Parameters

One of the primary differences between the gas dynamics and the energy balance approaches is that the gas dynamics approach makes use of both the stable and unstable stability parameters for all of the acoustic modes, while the energy balance approach uses only the unstable stability parameter for the unstable mode. While it is possible to reformulate the energy balance approach to utilize the stable parameters, the analysis shown in Figure 2 indicates that it might not be necessary. To evaluate the variation in stability as a function of the stable modes, for several test cases we kept the unstable mode stability parameter constant, and set the stable modes all to the same, positive number. The unstable stability parameter for the first mode was fixed at 100 s^{-1} , and the next 19 higher, stable modes were set to the same value: $-400, -412.5, -425, -450, -500, -600, -800, \text{ and } -1000 \text{ s}^{-1}$ (8 test cases). We performed several computations near -400 s^{-1} as we found the system went completely unstable when the higher mode stability parameters were closer to zero than -400 (see Figure 3). At first we thought this indicated a distinct difference between the gas dynamics and energy balance methods. However, according to Burnley, when time averaging is used to help solve the system of equations, there is a specific limit when the unstable mode is raised to high (our gas dynamics implementation uses time averaging). This corresponds to this situation in that the stable mode stability parameters are made to be too close to zero relative to the unstable parameter. Hence, we have recreated the stability limit shown in Figure 4 (from Burnley, Ref. 4). As the stable stability parameters are made more negative, their acoustic amplitudes quickly level out to constant values (Figure 3). Notably, the even mode amplitudes level out faster than the odd modes. While the mode amplitudes generally decrease with mode number, the 20th mode has a significant value. This is probably due to the combination of it having a both a smaller negative

stability parameter than usual (allowing it to be heard more easily), and because it is the last mode in the Fourier series (the truncated Fourier series error is concentrated in the last mode).

The most important factor that can be observed from Figure 3 is that as the stable modes achieve increasingly negative values, their amplitudes tend to plateau to constant values. In most motors, the higher modes tend to have significantly more negative stability parameters than the unstable fundamental mode. This implies that the stability is usually dominated by the unstable mode stability parameter, as the mode amplitudes of the stable modes tend to plateau. Reexamining the figure from Burnley (Figure 4b), the slope of the limit cycle amplitude vs. the unstable stability parameter is linear (until the time averaging fails), as was predicted by the energy balance approach.

Most test cases have monotonically decreasing (negative) stable stability parameters, which would at first make the test case in this section appear unusual. However, in the analysis of real motor, as shown in Section C, while the stable stability parameters reach a factor of ten larger than the unstable stability parameter, the stable stability parameters themselves plateau. The situation presented in this section is an extreme limit of this observation.

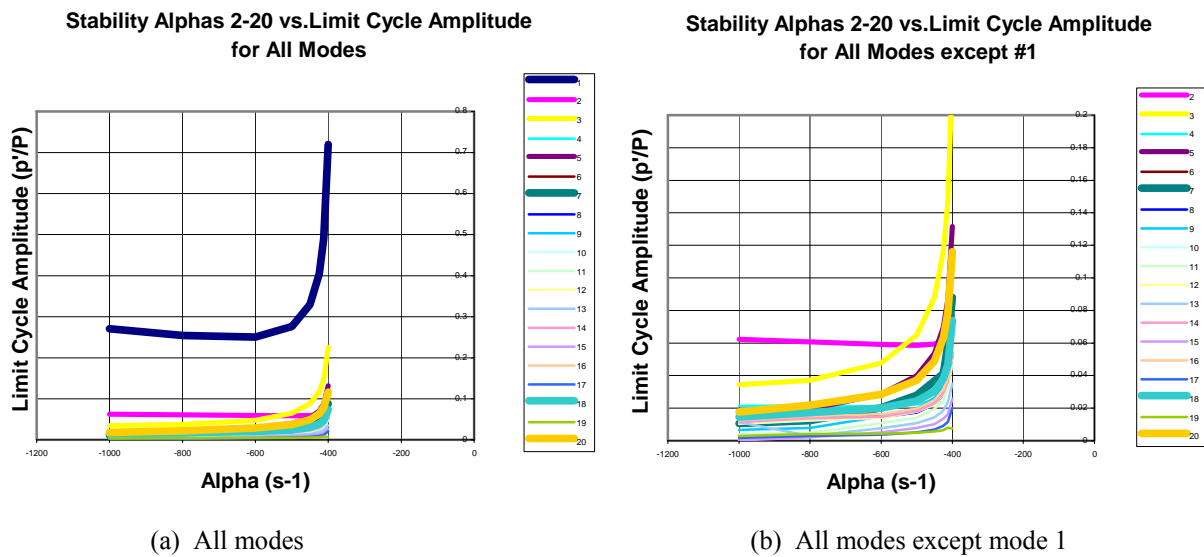


Figure 3. Comparison of Limit Cycle Amplitudes when Unstable Stability Parameter Fixed and Stable Stability Parameters Set to Same, Constant Values

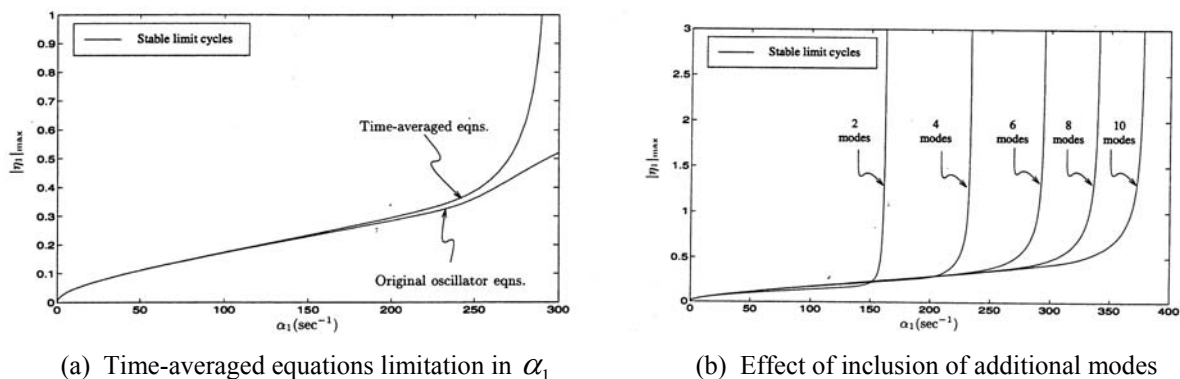


Figure 4. Limitation in Unstable Stability Parameter Due to Time-Averaging (Burnley)

B. Cylindrical Motor, Varied Stable Mode Stability Parameters

In a second set of test cases, we varied the unstable mode's stability parameter and kept the stable mode parameters constant. The unstable stability parameter was set to 5, 10, and 15 s^{-1} , while the stable modes (2-20) were set to -10 times the mode number (ie -20 for the second mode). It should be noted that when the unstable mode stability parameter was set to 20, the system was completely unstable (probably due to the time averaging). However, for the data shown, the increase in the unstable modes' amplitude is nearly linear as a function of the unstable mode stability parameter (Figure 5a), again agreeing with assumptions found in the energy balance approach.

To determine the effect of the overall magnitude of all of the stability parameters on the limit cycle amplitude, we repeated the analyses, changing the unstable mode parameters to 50, 100 and 150 s^{-1} , and the stable mode parameters were increased to -100 times the mode number. Comparison of Figure 5a and b demonstrate that the effect of multiplying all of the stability parameters by 10 was to raise the limit cycle amplitudes by a factor of 10.

We have included a direct comparison of each gas dynamics analysis with that derived from the energy balance approach, and as can be seen, the energy balance approach yields similar values for each test case.

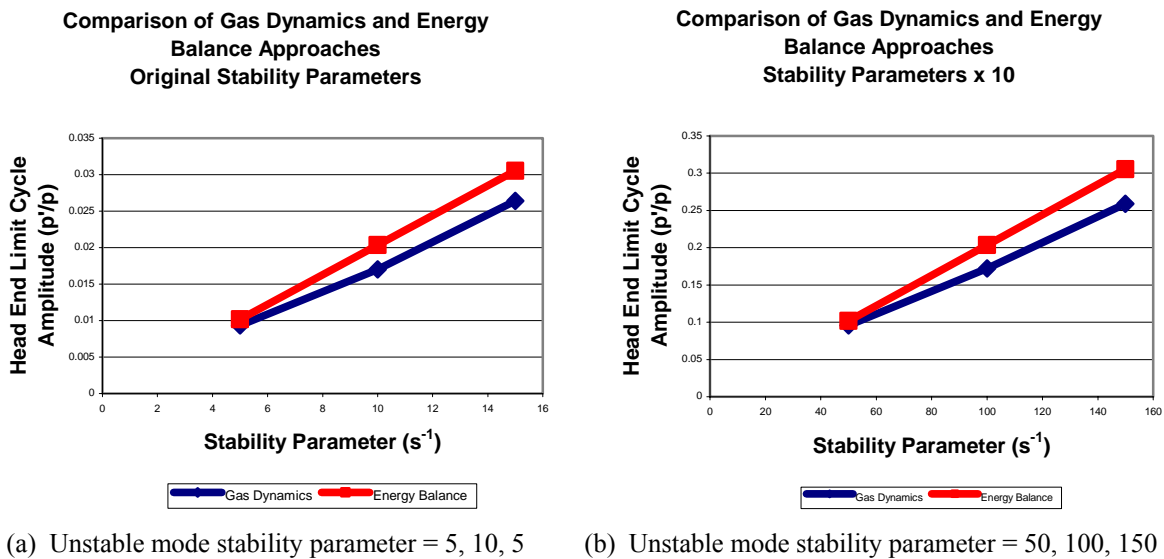
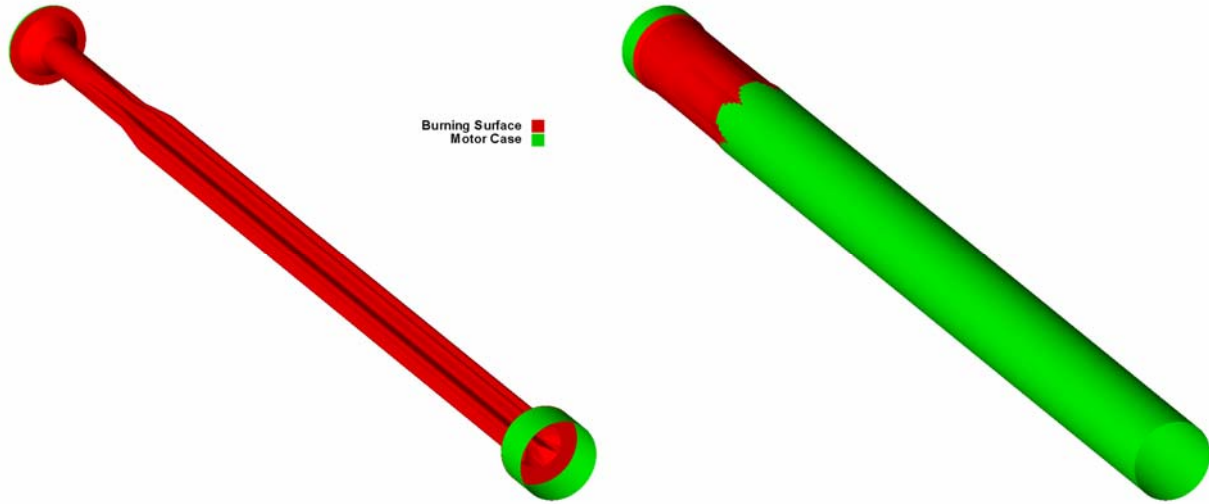


Figure 5. Comparison of Limit Cycle Amplitudes for Fixed Stable Mode Stability Parameters, Varying Unstable Mode Stability Parameters

C. Star-Aft Motor, Varied Number of Modes

Many solid rocket motors do not have cylindrical mode shapes, which tends to complicate the math. To examine the effect of a realistic motor, we evaluated a motor (Figure 6) which has a first mode instability late in its burn at $t=3.8s$ (Figure 7). The nonlinear analysis was performed using 10, 20 and 40 acoustic modes. It has been observed from prior nonlinear analyses that motors with axially varying grain designs establish standing wave forms that contain internal reflections.⁹ This motor exhibits an unusual repeated signal – a traveling square wave (Figure 8). This does not go immediately against the energy balance approach, as it does include a jump in the pressure that would indicate an entropy gain. As a demonstration of the effect of increasing the number of mode shapes, we doubled and quadrupled the number of modes. For the 10 mode case, the truncated Fourier series is evidenced by spurious waves that mar the overall solution. Each time the number of modes was doubled, the final overall waveform's amplitude of these spurious waves is halved, but the number of the spurious waves doubles. One

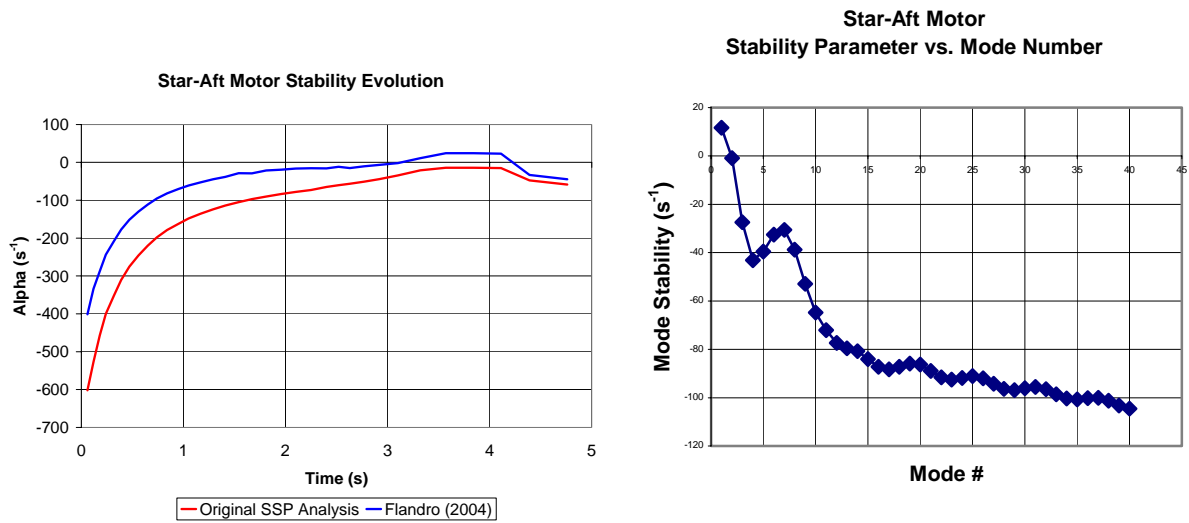
should also note that the wave amplitude is not symmetric about the y axis. High frequency experimental data from motor firings yield pressure traces that are often not symmetric about the DC pressure.



(a) Initial grain surface

(b) Grain surface at T = 3.8 seconds

Figure 6. Star-aft motor grain surface



(a) Stability of first acoustic mode as function of time

(b) Stability of first 40 modes at t = 3.8s

Figure 7. Star-Aft Motor Stability Analysis

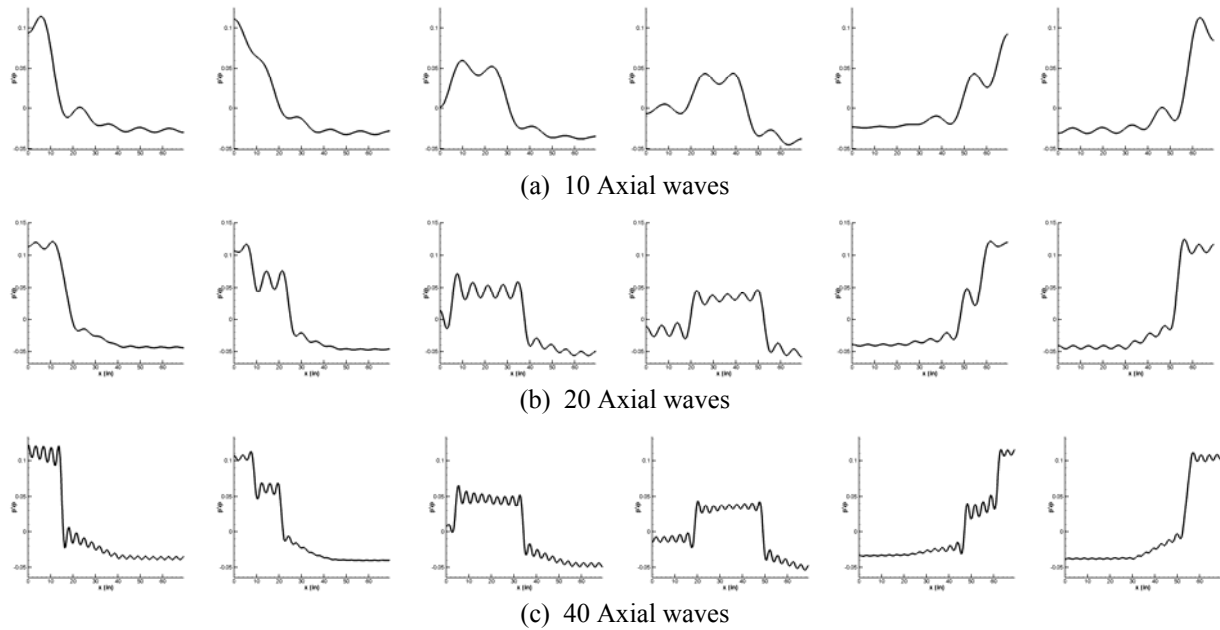


Figure 8. Traveling Square Wave in Star-Aft Motor for Varying Numbers of Axial Waves

IV. Conclusions and Further Work

SEA has encoded two nonlinear combustion stability modules into SPP. The gas dynamics methodology and the energy balance modules return similar values, as long as the series of stable stability parameters are significantly larger than the unstable stability parameter. We need to reformulate the energy balance approach to allow the individual mode shape amplitudes to vary with time. While this will increase the required computational time, it will allow for the evaluation of more complex acoustic motions.

The gas dynamics approach yields realistic overall acoustic motions that are not symmetric about the y-axis. Except for simple grain designs, the shape of these wave motions cannot be anticipated. It will be determined if the small size of the star-aft motor's second acoustic mode stability parameter is the source of the square wave formation.

Acknowledgments

We would like to thank Dr. Fred Blomshield (NAVAIR) for his ongoing support in the development of the SPP / SSP design code, and Douglas Coats (SEA) for funding the research and writing of this paper.

References

- ¹ Culick, F.E.C., and Yang, V., "Prediction of the Stability of Unsteady Motions in Solid Propellant Rocket Motors", Chapter 18 in *Nonsteady Burning and Combustion Stability of Solid Propellants*, Progress in Astronautics and Aeronautics, Vol. 143, 1992.
- ² Flandro, G.A., Majdalani, J., Fischbach, S.R., French, J.C., "Nonlinear Rocket Motor Stability Prediction: Limit Amplitude, Triggering and Mean Pressure Shift", 40th AIAA / ASME / SAE / ASEE Joint Propulsion Conference, AIAA-2004-4054, Fort Lauderdale, FL, July 2004.
- ³ French, J.C., Flandro, G.A., "Linked Solid Rocket Motor Combustion Stability and Internal Ballistics Analysis", 41th AIAA / ASME / SAE / ASEE Joint Propulsion Conference, AIAA-2005-3998, Tucson, AZ, July 2005.
- ⁴ Burnley, V.S., "Nonlinear Combustion Instabilities and Stochastic Sources", Thesis, California Institute of Technology, CA, 1996.
- ⁵ Flandro, G.A., "Approximate Analysis of Nonlinear Instability with Shock Waves", AIAA-82-1220, 18th Joint Propulsion Conference, Cleveland, OH, June 1982.
- ⁶ Flandro, G.A., "Energy Balance Analysis of Nonlinear Combustion Stability", *Journal of Propulsion and Power*, Vol 1, No 3, pp 210-221, May-June 1985.
- ⁷ Morfey, C.L., Temkin, S., "Unstable Combustion of Advanced Solid Propellants", Bolt, Beranek and Newman, Inc., Report No. 1547, Contract No. DA-18-001-AMC-1134(X), September 1967.
- ⁸ Baum, J.D., Levine, J.N., "Modeling of Nonlinear Combustion Instability in Solid Propellant Rocket Motors," AFRPL TR-83-058, February 1984.
- ⁹ French, J.C., "Non-Linear Combustion Stability Prediction of SRMs using SPP / SSP," 39th AIAA / ASME / SAE / ASEE Joint Propulsion Conference, AIAA-2003-4668, Huntsville, AL, July 2003.